Supplemental material for: "Instabilities at Frictional Interfaces: Creep Patches, Nucleation and Rupture Fronts"

Yohai Bar-Sinai[1], Robert Spatschek[2], Efim A. Brener[1,3] and Eran Bouchbinder[1]
[1] *Chemical Physics Department, Weizmann Institute of Science, Rehovot 76100, Israel*
[2] *Max-Planck-Institut für Eisenforschung GmbH, D-40237 Düsseldorf, Germany*
[3] *Peter Grünberg Institut, Forschungszentrum Jülich, D-52425 Jülich, Germany*

REDUCTION TO A QUASI-1D SYSTEM

Our goal here is to explain how the quasi-1D approximation used in Eq. (2) in the main text is systematically derived. The limit of small H, which is mentioned in the main text, means that $H \ll \ell$, where ℓ characterizes the length scale of variation of the fields in the x-direction. Under these conditions, the system can be described effectively as 1D [1, 2] and the procedure of the dimensional reduction is detailed below.

In most general terms, we solve the momentum-balance equation

$$\rho \ddot{\boldsymbol{u}} = \operatorname{div} \boldsymbol{\sigma} \ , \tag{S1}$$

for the elastic body described in Fig. S1, where Hooke's law is assumed to hold in the bulk. $\boldsymbol{\sigma}$ is Cauchy's stress tensor, ρ is the mass density and $\boldsymbol{u}$ is the displacement field.

The friction law outlined in the main text describes the shear stress applied by the interface to the elastic bulk. It serves as a boundary condition to Eq. (S1) at $y=0$. The other boundary conditions are (cf. Fig. S1)

- $y=0$: $\quad u_y=0 \quad$ and $\quad \sigma_{xy}=\tau$,
- $y=H$: $\quad \sigma_{yy}=\sigma \quad$ and $\quad \sigma_{xy}=\tau_d$,
- $x=0$: $\quad \partial_t u_x = v_d \quad$ and $\quad \sigma_{xy}=0$.

In actual calculations, we use systems that are sufficiently large in the positive x-direction to be effectively regarded as semi-infinite along this dimension.

We assume plane-strain conditions, under which Hooke's law takes the form

$$\begin{pmatrix} \sigma_{xx} \\ \sigma_{yy} \end{pmatrix} = \frac{2G}{1-2\nu} \begin{pmatrix} 1-\nu & \nu \\ \nu & 1-\nu \end{pmatrix} \begin{pmatrix} \epsilon_{xx} \\ \epsilon_{yy} \end{pmatrix} \ , \tag{S2}$$

where $\epsilon_{ij} = \frac{1}{2}\left(\frac{\partial u_i}{\partial x_j} + \frac{\partial u_j}{\partial x_i}\right)$ is the linearized strain tensor, G is the shear modulus and ν is Poisson's ratio. This linear equation can be solved for σ_{xx} in terms of ϵ_{xx} and σ_{yy} as

$$\begin{aligned} \sigma_{xx} &= \frac{2G}{1-\nu}\,\epsilon_{xx} + \frac{\nu}{1-\nu}\sigma_{yy} \\ &= \frac{2G}{1-\nu}\frac{\partial u_x}{\partial x} + \frac{\nu}{1-\nu}\sigma_{yy} \ . \end{aligned} \tag{S3}$$

Integrating the x-component of Eq. (S1) from $y=0$ to $y=H$ using Eq. (S3), the boundary conditions on σ_{xy} and assuming σ_{yy} is x-independent, we obtain

$$\begin{aligned} \int_0^H \rho \frac{\partial^2 u_x}{\partial t^2} dy &= \int_0^H \left(\frac{\partial \sigma_{xx}}{\partial x} + \frac{\partial \sigma_{xy}}{\partial y} \right) dy \\ &= \frac{2G}{1-\nu} \int_0^H \frac{\partial^2 u_x}{\partial x^2} dy + \tau_d - \tau \ . \end{aligned} \tag{S4}$$

In order to get a quasi-1D description, we define the effective 1D displacement field $u(x,t)$ as the mean displacement in the x-direction

$$u(x,t) = \frac{1}{H}\int_0^H u_x(x,y,t) dy \tag{S5}$$

and maintain that the y-component of Eq. (S1) is automatically satisfied in the main approximation with respect to H/ℓ. Physically, the last two conditions mean that for $H/\ell \ll 1$, the variation of u_x and σ_{yy} with y can be neglected (in the main approximation). Combining Eqs. (S4) and (S5) we obtain Eq. (2) in the main text

$$\rho H \ddot{u} = \frac{2GH}{1-\nu}\partial_{xx} u + \tau_d - \tau \ , \tag{S6}$$

with $\bar{G} = \frac{2G}{1-\nu}$. For our parameters (i.e. $\nu = 1/3$, see below) we obtain $\bar{G} = 3G$, which implies that the elastic wave-speed (there is only one wave-speed in this quasi-1D approximation) is larger than the bulk shear wave-speed

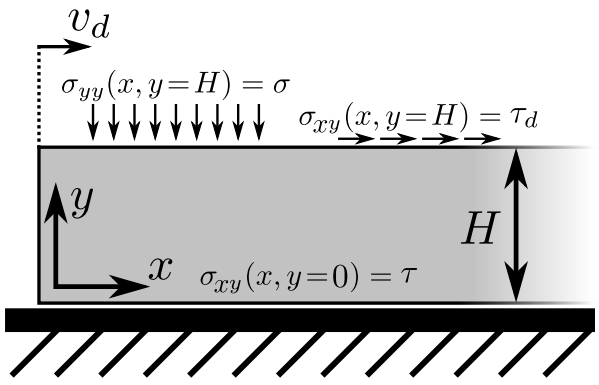

FIG. S1. Sketch of the system's geometry and loading configuration. Note that in addition to the system described in the main text, we allow here also for shear stresses to be applied at $y=H$.

and smaller than the bulk dilatational wave-speed. For plane-stress conditions (not used here), the result reads $\bar{G}=2(1+\nu)G$. Note also that we set $\tau_d=0$ in the main text.

Using Eq. (S3) the force per unit width (out-of-plane) exerted by the loading machine on the lateral boundary $x=0$ can be calculated as

$$\begin{aligned} f_d(t) &= -\int_0^H \sigma_{xx}(x=0,y,t)dy \\ &= -\bar{G}H\left.\frac{\partial u}{\partial x}\right|_{x=0} + \frac{\nu}{1-\nu}\int_0^H \sigma_{yy}dy \ , \end{aligned}$$

where the latter time-independent contribution was not included in $f_d(t)$ reported on in the main text. Finally, note that throughout our calculations we choose H (see below) such that $H \ll \ell$ under all circumstances considered in the main text. The question of when and how this quasi-1D formulation crosses over to the fully 2D formulation is interesting and important, and will be discussed elsewhere. In the next section we briefly discuss one aspect of it.

RELATION TO THE NUCLEATION SIZE IN 2D MODELS

To connect our analysis to some of the available literature on the nucleation size in 2D, we interpret L_c of Eq. (5) in the main text as the 1D nucleation size $L_c^{(1)}$, which is valid if $L_c^{(1)} \gg H$. The 1D limit is expected to break down when $L_c^{(1)} \sim H \sim L_c^{(2)}$, where $L_c^{(2)}$ is the critical nucleation size in 2D. Using the last relation in Eq. (5) of the main text, we obtain

$$L_c^{(2)} \sim \frac{GD}{\left|\frac{\partial \tau_{ss}}{\partial \log v}\right|} \tag{S7}$$

(here we do not distinguish between $\bar{G}$ and G), which is a known result, see for example [3, 4]. The 1D and 2D results can be combined into one expression $L_c = L_c^{(2)} f(H/L_c^{(2)})$, where $f(z)$ is a scaling function that satisfies $f(z)=\sqrt{z}$ for $z \ll 1$ and $f(z)=1$ for $z \gg 1$.

STEADY-STATE PROPAGATING FRONTS

As discussed in great detail in [1, 2], under constant stress boundary conditions steady-state rupture front solutions might emerge, see Fig. S2. These fronts exist when the homogeneously applied τ_d surpasses a threshold value and the system is bistable. The fronts connect a region which slips steadily at a velocity v_2 and in which $\phi = D/v_2$ to a region which slips at a velocity $v_1 \ll v_2$. Since v_1 is extremely small, we can practically

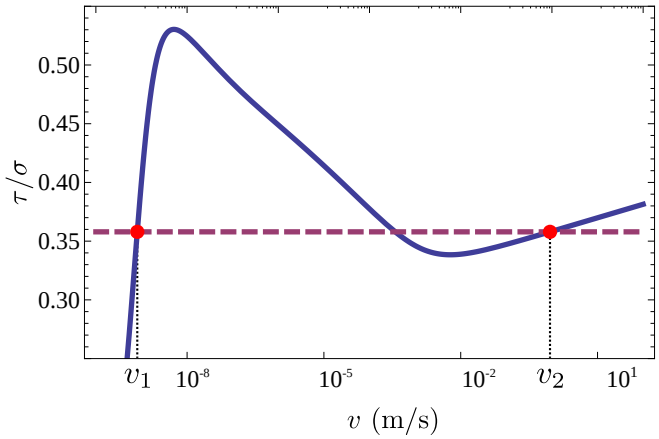

FIG. S2. Steady-state sliding friction vs. slip velocity v (solid blue line). The dashed horizontal line marks τ_d for the steady-state front shown in Figs. 3b-d of the main text.

treat this region as a "stick" (non-slipping) one and characterize it by $\phi=\phi_{stick}$, the age of the interface into which the front penetrates. Note that we *do not* typically consider the "true" steady-state of ϕ in the "stick" region, $\phi = D/v_1$, because it takes unrealistically long time to reach it (when v_1 is extremely small). For a given τ_d and ϕ_{stick}, the spatial distribution of the front's fields, as well as its propagation velocity, are uniquely determined.

In the main text, we described a fast event which emerges nonlinearly as the outcome of the linear instability of the creep patch (Fig. 3). The event features a steadily propagating rupture front, which penetrates a region with $\phi = 17.4$s and moves at $c = 902$m/s. As explained above, there exists a unique steady-state front with these characteristics, and this is the front shown in Figs. 3b-d of the main text. No other free parameters were used. The top-loading shear stress for this front, $\tau_d = 0.358\sigma$, is marked in Fig. S2, as well as the velocities v_1 and v_2, which correspond to this stress.

DIFFERENT VELOCITY-STRENGTHENING BEHAVIORS

In the main text we examine 3 types of behaviors at high slip velocities: (i) logarithmic velocity-strengthening, (ii) pure logarithmic velocity-weakening (iii) linear velocity-strengthening. In this section we briefly describe the origin of these possible behaviors, and the way they are introduced within our model.

Logarithmic velocity-strengthening

Logarithmic velocity-strengthening behavior stems from the short time cut-off ϕ^* in the aging dynamics, as explained at length in [2]. The contact area A is given

by

$$A(\phi) = \frac{\sigma}{\sigma_H}\left[1+b\log\left(1+\frac{\phi}{\phi^*}\right)\right] . \qquad \text{(S8)}$$

In steady-state sliding at velocity v the age of the interface is $\phi = D/v$. The fact that A decreases with increasing v is the source of the velocity-weakening behavior at low sliding velocities. However, at high sliding velocities D/v becomes negligible with respect to ϕ^*, implying that A in Eq. (S8) saturates at a finite value. This happens at $v_m \approx D/\phi^*$, where the system crosses over from logarithmic velocity-weakening to logarithmic velocity-strengthening because the viscous part of the friction stress, $\tau^{vis}(v,\phi) = \eta\, v^* A(\phi)\log(1+v/v^*)$, increases monotonically and logarithmically with v. The short-time cutoff was directly observed experimentally in PMMA [5] and other materials [6, 7], and the crossover from velocity-weakening to velocity-strengthening was observed in different materials by various authors, e.g. [8–15].

Pure velocity-weakening

The aforementioned crossover can be removed simply by using a constitutive equation for A which does not feature the short time cutoff, namely

$$A_{weak}(\phi) = \frac{\sigma}{\sigma_H}\left[1+b\log\left(\frac{\phi}{\phi^*}\right)\right] , \qquad \text{(S9)}$$

which is commonly used in the rate-and-state literature. This law was used to generate the pure velocity-weakening behavior shown by the dashed yellow line in Fig. 1b in the main text.

Linear velocity-strengthening

As explained above, using $\tau^{vis}(v,\phi) = \eta\, v^* A(\phi)\log(1+v/v^*)$ (together with Eq. (S8)) eventually determines the logarithmic velocity-strengthening behavior at high slip velocities. However, some studies reported on a much stronger than logarithmic velocity-strengthening behavior, possibly linear in v [10, 11, 14]. We believe this is an important, and possibly generic, feature of friction which we will discuss separately elsewhere. In the main text we explore the dramatic implications of this behavior by making $\tau^{vis}(v,\phi)$ linear in v above some value of v, as shown in the dotted red line in Fig. 1b in the main text.

DETERMINATION OF PARAMETERS FOR PMMA

We determined our realistic set of parameters for PMMA (a glassy polymer), an extensively used material in laboratory experiments. In particular, its interfacial elastic response [16], the existence of slow rupture fronts [5, 17–19], the variation of static friction coefficient with loading conditions [20], and additional properties [21–25] were carefully characterized.

The interfacial elastic response data of Fig. 2 in [16] indicated that $h\sigma_H/\mu_0$ is in the μm scale. The slope of the ageing data in Fig. 9 of [26] determines the value of $\frac{\mu_0 D\, b}{\sigma_H h} = 0.02$. The "direct effect" measurement in Fig. 4 of [26] determine $\eta v^*/\sigma_H = 0.005$. In [19], Fig. 3, the authors deduce that D is of the order of 1μm. With these constraints, and using known values of independently measured parameters such as μ, σ_H and ρ, we fitted all the aforementioned experimental data. Finally, we set $\sigma = 1$MPa, which is similar to the value used in [5, 19] and $H = 200\mu$m. This value of H ensures the validity of the quasi-1D approximation, though the latter approximation remains valid for much larger values of H (of the order of 1cm). The value $v_0 = 10^{-9}$m/s was chosen to be much smaller than any other velocity scale in the problem, and has no influence on the results we report. The parameters are summarized in table I.

G	3.1GPa	H	200μm
ρ	1200 Kg/m^3	v_d	10μm/s
v^*	10^{-7} m/s	μ_0/h	$3\cdot 10^{14}$ Pa/m
ϕ^*	0.33 msec	η	$27\cdot 10^{12}$ Pa sec/m
D	0.5μm	σ_H	540MPa
σ	1MPa	b	0.075
ν	1/3	v_0	10^{-9} m/s

TABLE I. Parameters of the model.

[1] E. Bouchbinder, E. A. Brener, I. Barel, and M. Urbakh, Phys. Rev. Lett. p. 235501 (2011).
[2] Y. Bar Sinai, E. A. Brener, and E. Bouchbinder, Geophysical Research Letters **39**, 2 (2012).
[3] J. R. Rice, Journal of Geophysical Research **98**, 9885 (1993).
[4] A. M. Rubin and J.-P. Ampuero, Journal of Geophysical Research **110**, 1 (2005).
[5] O. Ben-David, S. M. Rubinstein, and J. Fineberg, Nature **463**, 76 (2010).
[6] J. H. Dieterich, Journal of Geophysical Research **84**, 2161 (1979).
[7] M. Nakatani and C. H. Scholz, Journal of Geophysical Research **111**, B12208 (2006).
[8] T. Shimamoto, Science **231**, 711 (1986).
[9] B. D. Kilgore, M. L. Blanpied, and J. H. Dieterich, Geophysical Research Letters **20**, 903 (1993).
[10] J. D. Weeks, Journal of geophysical research **98** (1993).
[11] F. Heslot, T. Baumberger, B. Perrin, B. Caroli, and C. Caroli, Physical Review E **49**, 4973 (1994).
[12] A. Tsutsumi and T. Shimamoto, Geophysical research letters **24**, 699 (1997).

[13] Z. Reches and D. A. Lockner, Nature **467**, 452 (2010).
[14] F. Ferri, G. Di Toro, T. Hirose, R. Han, H. Noda, T. Shimamoto, M. Quaresimin, and N. de Rossi, Journal of Geophysical Research **116**, 1 (2011).
[15] G. Di Toro, D. Goldsby, and T. E. Tullis, *Unpublished data*.
[16] P. Berthoud and T. Baumberger, Proceedings of the Royal Society of London. Series A: Mathematical, Physical and Engineering Sciences **454**, 1615 (1998).
[17] S. M. Rubinstein, G. Cohen, and J. Fineberg, Nature **430**, 1005 (2004).
[18] S. M. Rubinstein, G. Cohen, and J. Fineberg, Physical Review Letters **98**, 1 (2007).
[19] O. Ben-David, G. Cohen, and J. Fineberg, Science **330**, 211 (2010).
[20] O. Ben-David and J. Fineberg, Phys. Rev. Lett. **106**, 254301 (2011).
[21] P. Berthoud and T. Baumberger, Europhysics Letters (EPL) **41**, 617 (1998).
[22] P. Berthoud, T. Baumberger, C. GSell, and J.-M. Hiver, Physical Review B **59**, 14313 (1999).
[23] T. Baumberger and P. Berthoud, Physical Review B **60**, 3928 (1999).
[24] L. Bureau, T. Baumberger, and C. Caroli, Physical Review E **62**, 6810 (2000).
[25] L. Bureau, T. Baumberger, and C. Caroli, The European physical journal. E, Soft matter **8**, 331 (2002).
[26] T. Baumberger and C. Caroli, Advances in Physics **55**, 279 (2006).